npj | materials degradation

Article

Published in partnership with CSCP and USTB

https://doi.org/10.1038/s41529-024-00471-9

Corrosion behavior of austenitic stainless steel and nickel-based welded joints in underwater wet welding

Leandro Vaccari ✉, Thomas Scheithauer, Ivan Lendiel, Jan Klett, Thomas Hassel & Hans Jürgen Maier

Marine structures such as ports, bridges, pipelines, vessels, and platforms are an essential part of modern infrastructure, where the use of higher-strength steel provides savings in logistics and construction. However, the repair of higher-strength steels can be challenging, especially underwater. Wet shielded metal arc welding is the most widely used and least expensive method for underwater welding repairs, but is very susceptible to hydrogen-induced cracking. Thus, researchers and welding engineers aim to reduce the amount of hydrogen in the weld material. Recent success has been achieved through the use of austenitic welding consumables, such as austenitic stainless steel and nickel-based electrodes. The use of these consumables drastically reduces the amount of diffusible hydrogen in the weld metal. However, these austenitic materials usually have different corrosion potential as compared to the structural steel the weld beads are applied to. This creates the risk of severe galvanic corrosion. In the presented study, the corrosion behavior of welds created with austenitic stainless steel and nickel-based electrodes were studied. Samples were aged for 1.5 years in the Baltic Sea. Simultaneously, the effectiveness of corrosion protection systems such as coating and Impressed Current Cathodic Protection (ICCP) were evaluated. Localized corrosion occurred in the heat-affected zone when austenitic electrodes were used in the corrosive environment. The localized corrosion depth after 1.5 years in the Baltic Sea and in the salt spray layer was approximately 250 µm and 390 µm, respectively. The ICCP system and the use of a coating were effective in preventing localized corrosion. The low pitting corrosion density of $2.5 \times 10^3\,m^{-2}$ corresponds to grade A1 according to the standard and was found to be negligible as compared to the localized corrosion in the heat-affect zone.

The field of underwater arc welding can be divided into two major groups referred to as dry underwater welding and wet underwater welding. Underwater dry welding uses a habitat that isolates the process zone from the surrounding water. Thus, this technique is associated with high costs. In underwater wet welding, the electrode, the workpiece, and the arc are in direct contact with the water. Wet welding is usually performed as shielded metal arc welding (SMAW), or, in scientific studies, by using flux-cored arc welding[1,2].

The direct contact of the welding area with water creates several challenges: The rapid cooling tends to cause the formation of martensitic and bainitic phases in the heat-affected zone (HAZ), resulting in microstructures with high hardness[3]. For underwater wet welding, the critical cooling time may vary in a range of 1–6 seconds ($\Delta t_{8/5}$)[3,4]. In addition, the contact of the arc with water results in dissociation, ionization, and recombination of oxygen and hydrogen.

Fractions of these gases are absorbed into the weld material[1,5–7], and part of the hydrogen diffuses into the mentioned hard microstructures, where it can lead to cold cracking. The total amount of dissolved hydrogen, the residual stresses, and the hardness of the microstructure in the HAZ are factors, directly correlated to the likelihood of the formation of cold cracks[8–10].

Institut für Werkstoffkunde (Materials Science), Leibniz Universität Hannover, An der Universität 2, 30823 Garbsen, Germany.
✉e-mail: vaccari@iw.uni-hannover.de

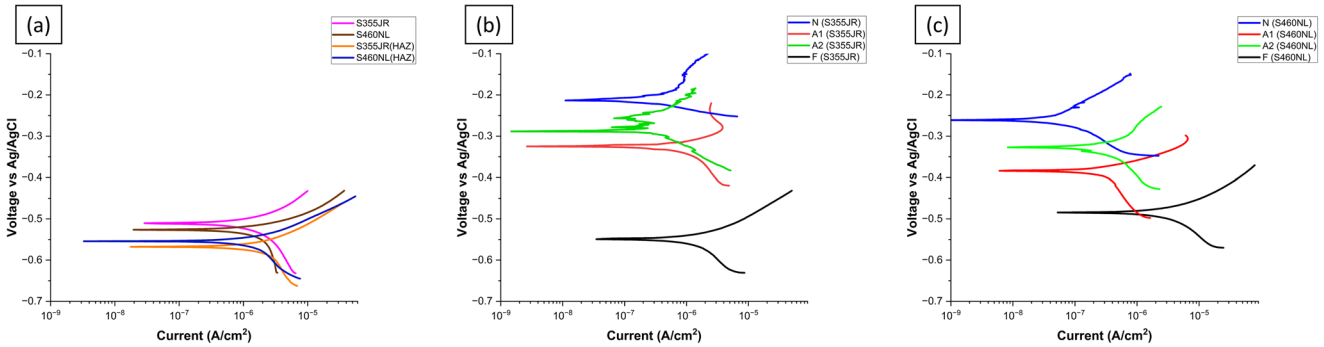

Fig. 1 | Polarization curves. a base materials and heat-affected zones, **b** austenitic and nickel-based weld bead on S355JR, **c** on S460NL.

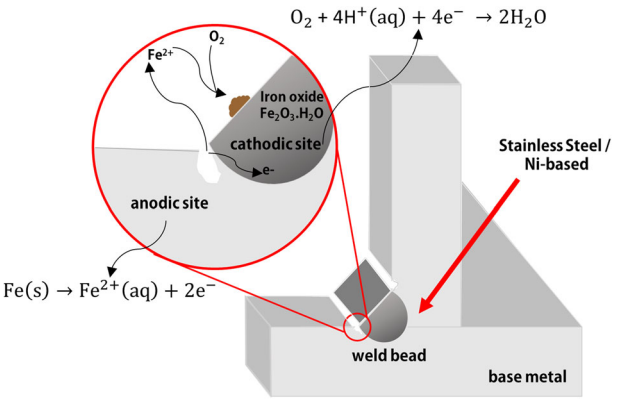

Fig. 2 | Localized corrosion. Schematic representation of the corrosion processes localized at the HAZ when using austenitic consumables.

According to standard ISO EN 2560, the amount of diffusible hydrogen in dry welding must not exceed 15 ml/100 g[11,12], or additional pre-, and/or post-heating must be performed in order to control the risk of cold cracks in the weld microstructure. However, the amount of diffusible hydrogen found in wet welded samples using ferritic stick electrodes generally is in the range of 30–100 ml/100 g[8,13–17]. An alternative that has been shown to be efficient in reducing the amount of diffusible hydrogen in the weld metal is the use of austenitic stainless steel or nickel-based electrodes, which allow for a reduction of the diffusible hydrogen content in the weld metal to values ranging from 5 to 25 ml/100 g[14]. This reduction can be attributed to the fact that the solubility of diffusible hydrogen is significantly higher in metals with face-centered than in body-centered crystalline structures[18]. Additionally, the diffusion coefficient of hydrogen in austenitic metal is lower compared to ferritic metal. This leads to significantly reduced diffusion of hydrogen from the weld bead to the heat-affected zone at room temperature, consequently reducing the risk of hydrogen-induced cold cracking there.

However, in flowing seawater austenitic stainless steels and nickel-based alloys have a corrosion potential (E_{corr} (vs. Ag/AgCl electrode)) of at least 200 mV above the corrosion potential of structural steels. This may cause the formation of a critical galvanic corrosion cell[19,20]. For galvanic corrosion to occur, some factors are simultaneously required, such as electrical contact between two metals with a corrosion potential above 200 mV in the presence of an electrolyte[21,22]. At the anode the metal dissolves in the first step as Fe^{2+} [20,23–25]. In the cathodic area, corrosion products are usually formed in a cathodic reaction[20].

Additionally, stainless steel may suffer pitting corrosion when aged in marine environments. The presence of halides (e.g., Cl^-) can cause the breakdown of the protective chromium oxide layer of stainless steel and nickel-chromium alloys as used in the present study. This breakdown in the protective layer generates differences, in corrosion potential, creating a corrosion cell within the austenitic phase itself[26,27]. A method of evaluating pitting corrosion susceptibility is through the pitting resistance equivalent number (PREN), shown in Equation 1 and Eq. 2[20,28].

The ways to prevent corrosion in marine environments is through the use of barrier coatings and/or cathodic protection systems[22]. Underwater coatings are used for the protection of submerged surfaces against corrosion and other forms of degradation caused by the environment. In such a weld joint, the coating acts as a barrier, in order to avoid the contact of the weld metal and base material with the electrolyte (seawater), thus avoiding the formation of galvanic corrosion[22,29]. Cathodic protection is another well-known technique for preventing corrosion on structures. The metal to be protected acts as the cathode in the electrochemical reaction, which prevents the metal from being corroded[30]. There are two main types of cathodic protection: sacrificial anode cathodic protection and impressed current cathodic protection (ICCP). ICCP is a method that uses an external power source to apply an electric current to a metal structure to prevent corrosion[30,31]. The ICCP systems consist of three main components: an anode, a rectifier, and a reference electrode[30,32].

The ICCP method as a control of the corrosion process was evaluated in the present study. Specifically, the corrosion behavior of dissimilar joints between weld seams made of austenitic stainless steel and nickel-based alloys with the structural steels S355JR and S460NL was evaluated. For this evaluation, welded samples were submerged in the Baltic Sea for one and a half year, and in parallel samples were tested in a salt spray chamber. Corrosion testing in the Baltic Sea brings the conditions as close as possible to future applications, and allows for including sea currents, temperature, microorganisms, etc. in the evaluation[33–35]. Part of the samples was coated to prevent galvanic corrosion. Additionally, an ICCP system was evaluated in the lab environment. The corrosion potential, localized corrosion, and pitting corrosion were evaluated. The overall aim of the study was to analyze and understand the corrosive behavior of welded joints between austenitic stainless steels or nickel alloys and structural steels, and to evaluate methods of protection against galvanic corrosion.

Results and discussion

Electrochemical analysis

The corrosion potential (E_{corr}) was measured on all the samples. As the base materials S355JR and S460NL are low alloyed structural steels, the E_{corr} was around −500 mV in both cases (E_{corr} −510 ± 10 mV for S355JR and E_{corr} −525 ± 10 mV for S460NL). The polarization curves are shown in Fig. 1a.

In the welding process, the HAZ is often the most sensitive part of a welded joint[36,37]. The heat input promotes grain growth, generating the appearance of coarse grains, as well as, in ferritic/pearlitic structural steels the formation of martensitic and bainitic phases. Thus, the HAZ typically has the highest hardness, lowest ductility, and lowest corrosion resistance[24,38–40]. As shown in Fig. 1a, it can be seen that for both base metals, the HAZ featured the lowest corrosion potentials (E_{corr} −565 ± 20 mV for S355JR and E_{corr} −555 ± 15 mV on S460NL).

Subsequently, polarization curves of the weld metal were recorded, for the different welding electrodes used (Fig. 1b, c). On both base metals, the

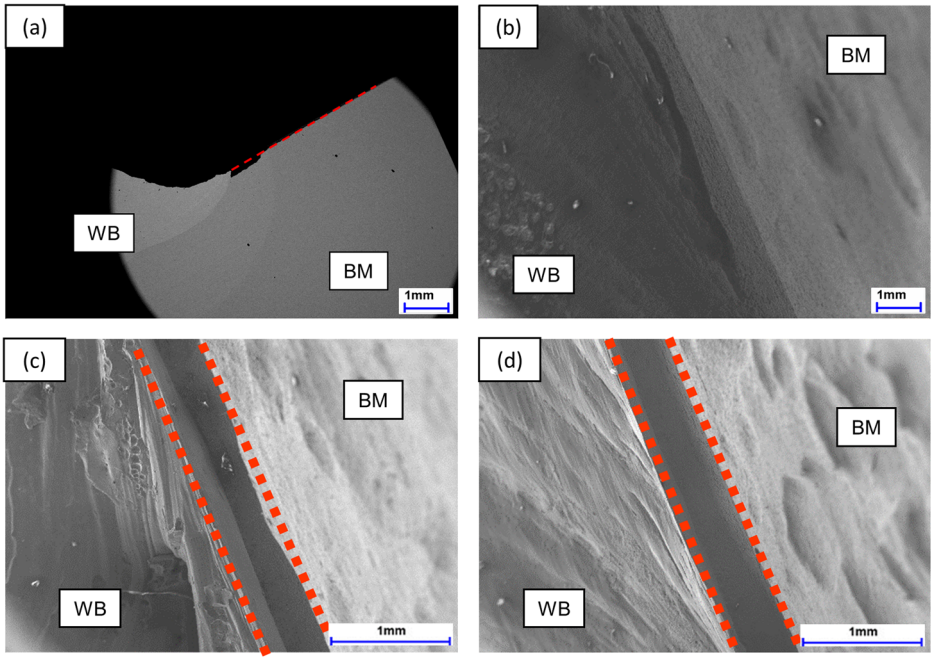

Fig. 3 | Localized corrosion. a cross section of A1 electrode **b**–**d**: top view of contact zone between weld bead and base material: Weld beads **b** F electrode **c** A2 electrode **d** N electrode showing localized corrosion on **a**, **c**, **d**. (BM base material / WB weld bead).

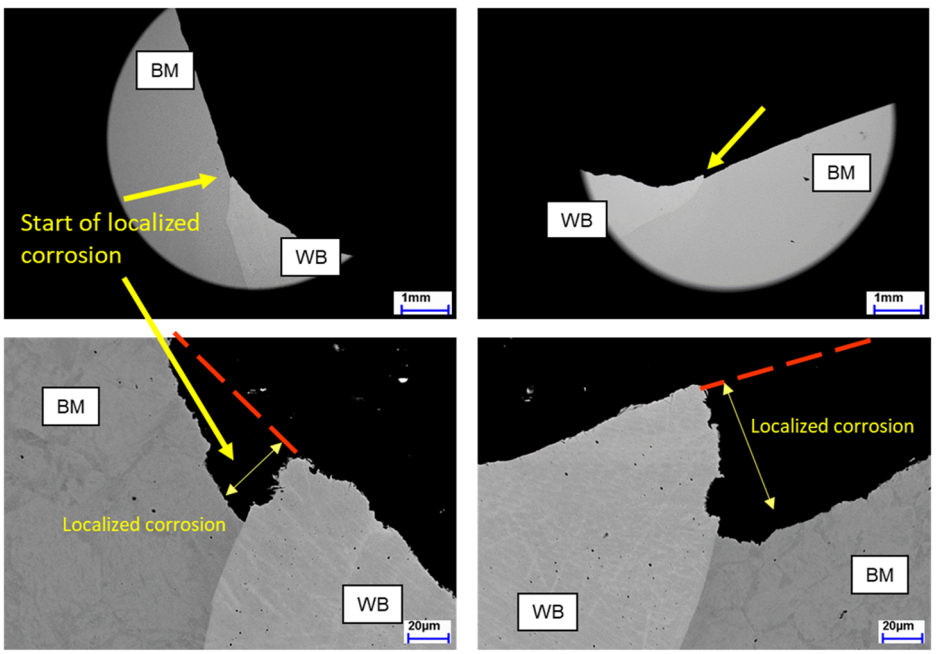

Fig. 4 | Localized corrosion. After 60 days in the Baltic Sea (A2 (S460NL)) (BM base material / WB weld bead).

weld metal of the Ni-base electrode (N) showed the lowest E_{corr} values (E_{corr} −215 ± 5 mV on S355JR and E_{corr} −265 ± 15 mV on S460NL).

Using the Schaeffler diagram, the structure of the N-weld metal (after dilution with the base metal) for both base metals should correspond to a highly stabilized austenitic steel[14]. The electrodes A1 (E_{corr} −290 ± 15 mV on S355JR and E_{corr} −330 ± 15 mV on S460NL), and A2 (E_{corr} −325 ± 5 mV on S355JR and E_{corr} −385 ± 10 mV on S460NL) presented similar E_{corr} due to the similar chemical composition between the electrodes (both form austenitic steel weld metal on the used base metals[14]). The electrode F (E_{corr} −550 mV ± 20 on S355JR and E_{corr} −525 ± 20 mV on S460NL) showed similar E_{corr} to the base metal due to its ferritic microstructure (Fig. 1b, c). Galvanic corrosion occurs when the corrosion potential difference (E_{corr} (vs Ag/AgCl electrode)) between metals is >200 mV, provided that there is an electrolyte and electrical contact between the parts[21,41]. Based on the polarization curves all the factors for galvanic corrosion to occur are present if seawater is added as an electrolyte. The highest E_{corr} is reached by the stick electrode N welded on S355 (E_{corr} −215 mV). In this case, the HAZ acts as the anode, and the austenitic areas act as the cathode.

Comparing the corrosion potentials of the base material, it can be seen that the N, A1, and A2 electrodes had a reduction in E_{corr} by ≈−50 mV when welded on S460NL as compared to ones on S355JR (Fig. 1b, c). This reduction is due to the change in composition of the weld bead, due to the different compositions of the base metals. However, even with this reduction, the corrosion potential is still large enough for galvanic corrosion to occur.

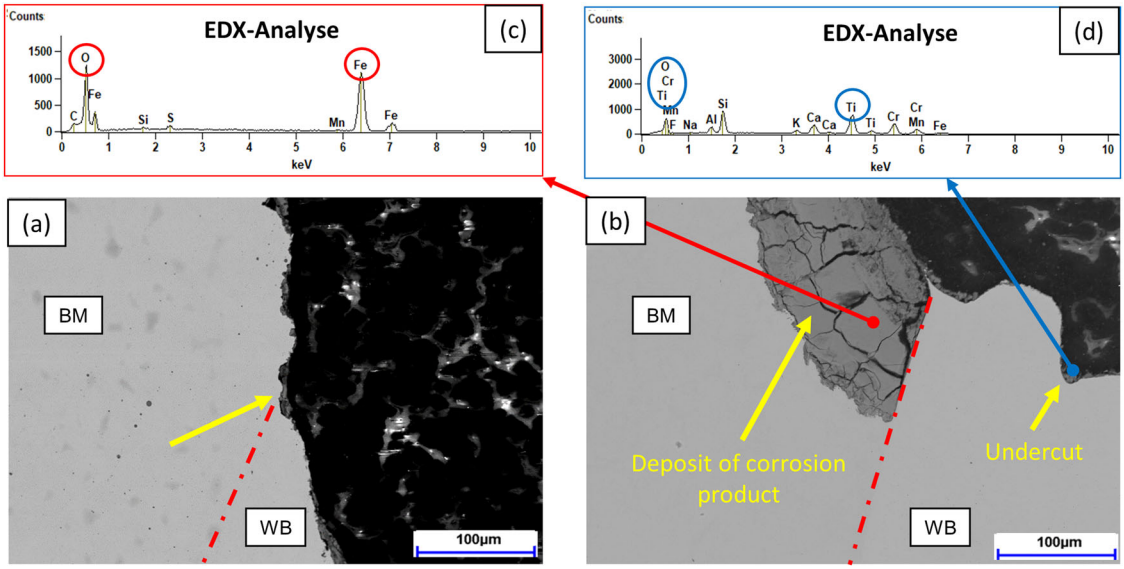

Fig. 5 | Samples after 1 year aging. a—F electrode **b**—N electrode **c** EDS analysis of the corrosion product **d**—EDS Analysis of the slag (BM base material / WB weld bead).

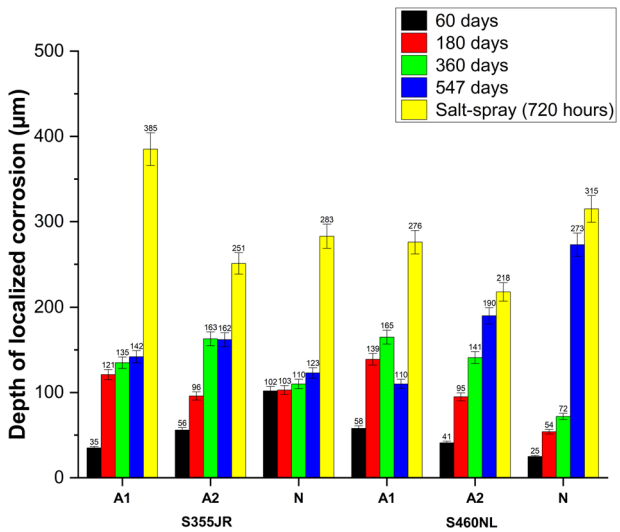

Fig. 6 | Depth of localized corrosion. Samples welded with austenitic stainless steel and nickel-based electrodes after aging in the Baltic Sea.

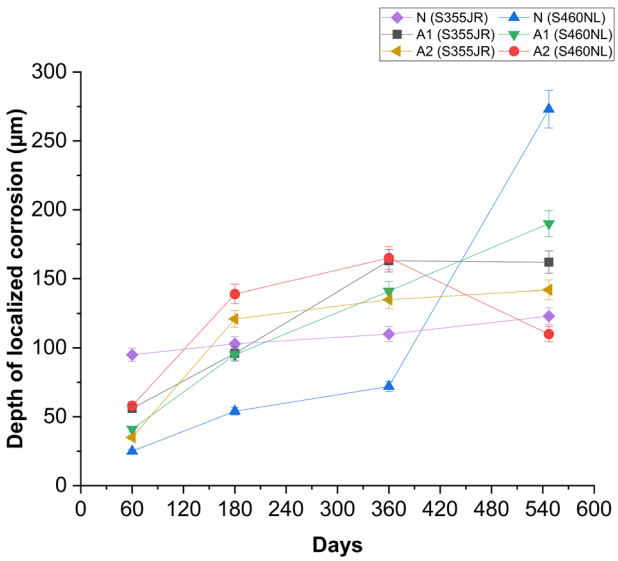

Fig. 7 | Depth of localized corrosion. Samples welded with austenitic stainless steel and nickel-based electrodes after aging in the Baltic Sea.

In all cases, the different E_{corr} values of the weld metal and the HAZ provide the driving force for an accelerated corrosion attack, thus leading to localized corrosion at the anode (HAZ).

Localized corrosion

After testing in the salt spray chamber, localized corrosion was found on samples welded with the electrodes N, A1, and A2. No localized corrosion was observed on the samples where the F electrode was used, due to the corrosion potential being similar to the base metal. The localized corrosion can be explained by the creation of a localized galvanic cell, due to the difference in corrosion potential as shown in Fig. 2. Localized corrosion is a form of corrosion that leads to the formation of small, deep pits that weakens the metal and potentially cause failure. For detailed evaluation, the samples subjected to 720 hours of testing in the salt spray chamber were analyzed in the scanning electron microscope (SEM). Figure 3 shows the corrosion attack at the contact point between the HAZ and the weld metal.

The localized corrosion depth was evaluated for samples deposited in the salt spray chamber for 720 hours as well as for samples aged for 60 days, 180 days, 360 days, and 547 days in the Baltic Sea. To measure the localized corrosion depth, cross-sections were cut from the specimens and then analyzed in the SEM. For the measurements, the side of the weld bead was taken as the starting point. The area marked by the red line represents the point on the base metal before the corrosion process (Fig. 4).

One of the samples using A1 electrode, aged at the Baltic Sea for 60 days, starting November 2021, is shown in Fig. 4. Note that on one side of the HAZ, the depth of localized corrosion was ≈40 µm, and on the other side ≈70 µm. This same behavior was observed in the other samples when the electrodes N, A1, and A2 were used.

Figure 5 compares the samples after 1 year of aging in the Baltic Sea. On the left side (a), it is shown that there was no localized corrosion when using the F electrode due to the similar potential difference to the base material.

On the right side (b), it is shown that there was localized corrosion when using the N electrode, where the depth of localized corrosion penetration was ≈110 µm. A weld defect (undercut) can also be seen in the weld bead.

The EDS analysis in Fig. 5c, revealed that the starting material acted as the anode in the galvanic reaction and was finally transformed into iron oxide, while the weld bead acted as the cathode (Fig. 2). The spectra in Fig. 5d shows the presence of a significant amount of elements such as Ti, which cannot be explained based on the composition of the base metals. In this context, it is important to note that rutile-basic type coated electrodes were used, and some of the slags remained in the material after the welding process, which is then detected in the EDS spectra.

The localized corrosion depth of the samples with each of the A1, A2, and N electrodes, on both base materials is shown in Figs. 6 and 7. In general, an increase in corrosion depth with an increasing duration of aging can be observed.

Pitting corrosion

The so-called pitting corrosion equivalent number (PREN) empirically predicts whether the specimen will suffer pitting corrosion based on its chemical composition. To determine the chemical composition, the cross-sections of the samples were examined using EDS. Based on the determined chemical composition, the PREN value was calculated, where Equation 1 and Eq. 2 are used for stainless steel and nickel-based alloys, respectively[20,28]. Using the determined chemical compositions, the formula for the pitting corrosion number was applied, and the PREN was determined. According to literature, steels with a PREN above 40 do not suffer pitting corrosion, as is the case with super duplex steels[26–28].

$$PREN_{\text{Stainless Steel}} = \%Cr + 3.3x\%Mo + 16x\%N \quad (1)$$

$$PREN_{\text{Ni}} = \%Cr + 1.5(\%Mo + \%W + \%Nb) \quad (2)$$

The composition analysis was performed point by point along a 5 mm long line running from the base metal to the top of the weld bead. The graphs in Figs. 8–10 demonstrate the steep gradient in chemical composition obtained with the A1, A2, and N electrodes welded on the S355JR and S460NL steels.

Using the average chemical composition obtained from the weld bead (Figs. 8–10), the PREN was calculated, cf. Table 1.

Both the DIN 11463 and the ASTM G46 standards describe the pitting evaluation process and specify the same approach to evaluate pitting density, size, and depth[42,43]. In the samples, small pits were found with a width of ~250 µm, with an elliptical shape according to the shape classification.

The number of pittings in the samples removed after 180 and 360 days from the Baltic Sea was counted on the whole surface of the weld beads, and the surface area of the pittings was measured. The density was converted into pittings/square meter and compared with the table provided in the standard. The pitting density was graded as A1 (2.5×10^3 m^{-2}), the size less than B1 (0.5 mm^2), and the depth as C1 (0.4 mm), according to the standard.

The low number of pittings (A1—2.5×10^3 m^{-2}), can be explained by the high PREN, which also indicates that the PREN can be used to predict the behavior of underwater welds. Moreover, it is known that the Baltic Sea has a low salt concentration of ≈5 g per kg of water, whereas other seas reach values up to 35 g per kg of water[44]. This appears to be another factor that influenced the amount of pittings. Overall, the localized corrosion in the HAZ was more severe than the pitting corrosion.

Coating

The coating was applied and cured underwater, simulating the process a professional diver would perform in the open sea. The coated specimens welded with A1, A2, N, and F electrodes were evaluated after 60 days, 180 days, 360 days, and 547 days of aging in the Baltic Sea. Overall, no localized corrosion was found in any of the specimens, as shown in Fig. 11. This shows that the use of coating can be an alternative to using austenitic and nickel-based stainless-steel electrodes in wet underwater welding provided that the coating will not get damaged during operation.

Impressed current cathodic protection

The constructed ICCP system was also effective against corrosion on the samples, as no degradation was observed after 120 days. The average temperature during 120 days of exposure was 25.4 °C. In tests without cathodic protection, an orange coloration from the iron oxide was observed after a few hours, whereas this was not observed in the tests with the ICCP system active. Two days after starting the tests, the potential stabilized at −1099 mV with a current of 0.01 A, and remained constant until the end of the 120 days test period. The pH of the artificial seawater solution before the tests was 8.1 and after 120 days it was 8.3, where the slight increase in pH can be explained by the reaction at the cathode generating ions (OH^-), which is typical when using ICCP system[45,46]. The specimens were subjected to metallographic analysis as shown in Fig. 12 and no evidence of localized corrosion found any case. It can be concluded that the ICCP system is effective in preventing corrosion when austenitic electrodes are used. Therefore, the use of austenitic stainless steel and nickel-based electrodes for underwater welding can be an option for cathodically protected structures such as ships, monopiles, and offshore structures.

A layer was detected on the samples, which based on composition corresponds to calcium carbonate. This typically precipitates in artificial seawater when using an ICCP system[47,48]. The cathodic reduction of oxygen produces local alkaline surface conditions, which precipitates $CaCO_3$ and $Mg(OH)_2$[35]:

$$Ca^{2+} + HCO_3^- + OH^- \rightarrow H_2O + CaCO_3 \quad (3)$$

$$Mg^{2+} + 2OH^- \rightarrow Mg(OH)_2 \quad (4)$$

In this study, the corrosion behavior at the joint between structural steel, austenitic stainless steel, and nickel alloy weld seams formed by underwater welding was investigated. The main results can be summarized as follows:

- Localized corrosion occurred in the HAZ resulting from the welding process. The depth of localized corrosion increased with exposure time. The maximum corrosion depth was ≈250 µm after one and a half years of exposure in the Baltic Sea and ≈385 µm after 720 hours in a salt spray chamber.
- The differences in severity of corrosion attack was found to be only minor between the different substrate/weld electrode combinations. Moreover, the localized corrosion in the HAZ could be prevented through the use of an epoxy coating, which can be applied by divers underwater. Thus, electrode materials can be selected with a focus on other issues such as reducing the amount of diffusible hydrogen in the weld.
- The use of an ICCP system was also efficient in preventing material degradation by corrosion.
- The austenitic stainless steel and nickel-based electrodes had corrosion potentials between −215 mV and −385 mV, while the base material and HAZ had corrosion potentials ranging from −510 mV to −570 mV. Thus, in the galvanic reaction, the austenitic stainless steel and nickel-based electrodes acted as the cathode and the base materials as the anode.
- There was a low amount of pitting (2.5×10^3 m^{-2}) on the samples exposed for one and a half years in the Baltic Sea.

Methods

Welding station, base material, and electrodes

The samples were welded using the SMAW process, and fillet welds were made, in order to simulate possible field applications. The experiments were carried out in a welding tank with dimensions 2 m × 3 m × 1 m. The movement of the x and y axis was done fully automated at constant speed[13]. The movement of the z axis was done by controlling the arc voltage. With

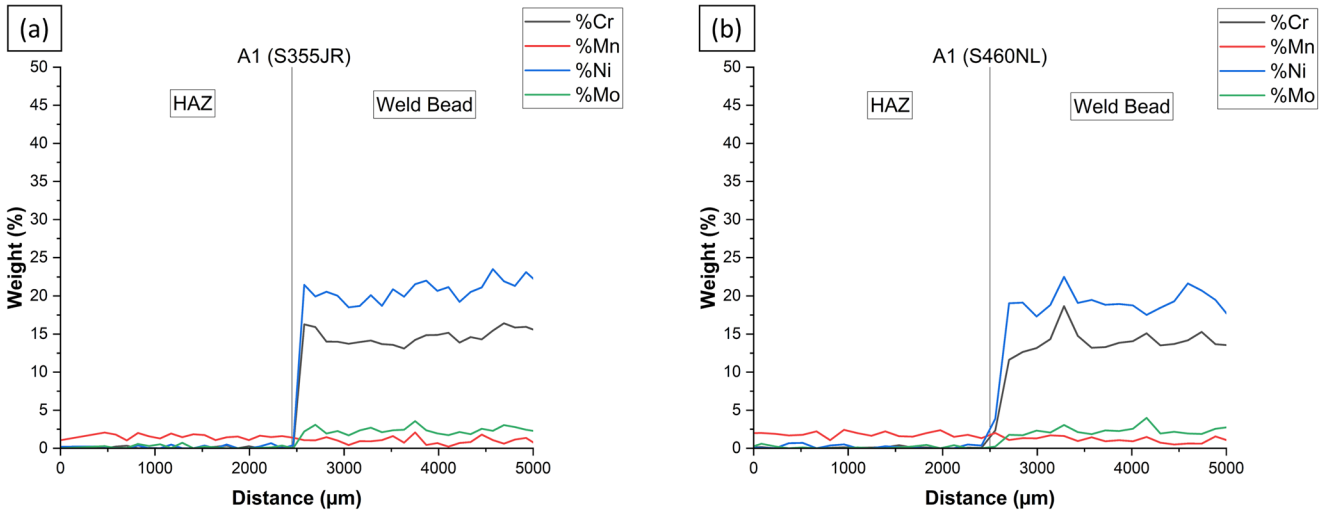

Fig. 8 | EDS line scan. Data across the weld bead/HAZ interface generated with the A1 electrode **a** on S355JR, **b** on S460NL.

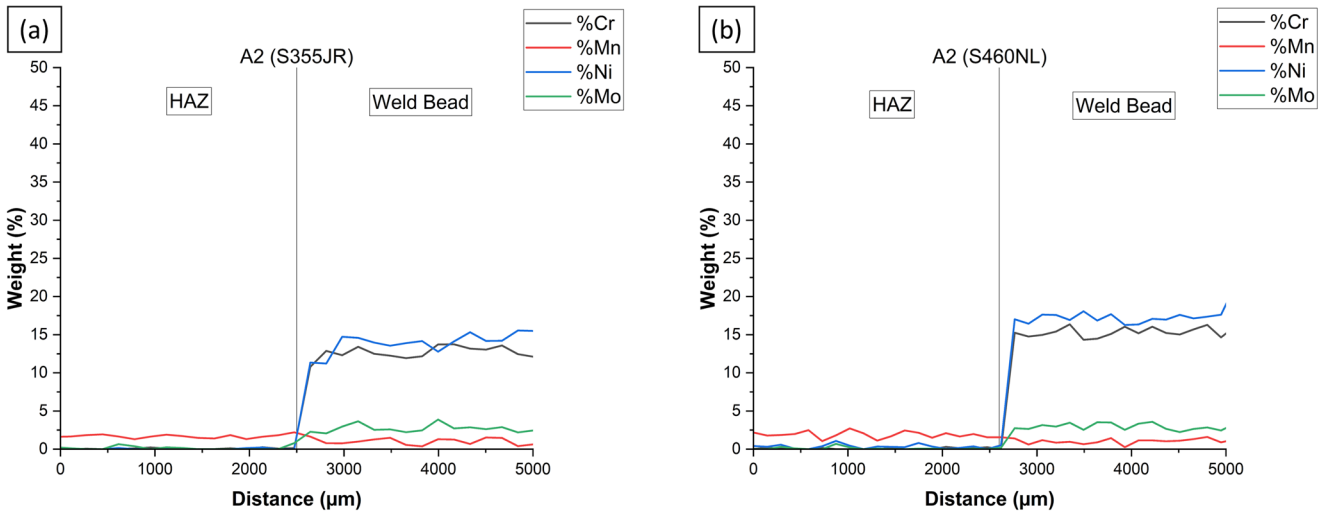

Fig. 9 | EDS line scan. Data across the weld bead/HAZ interface generated with the A2 electrode **a** on S355JR, **b** on S460NL.

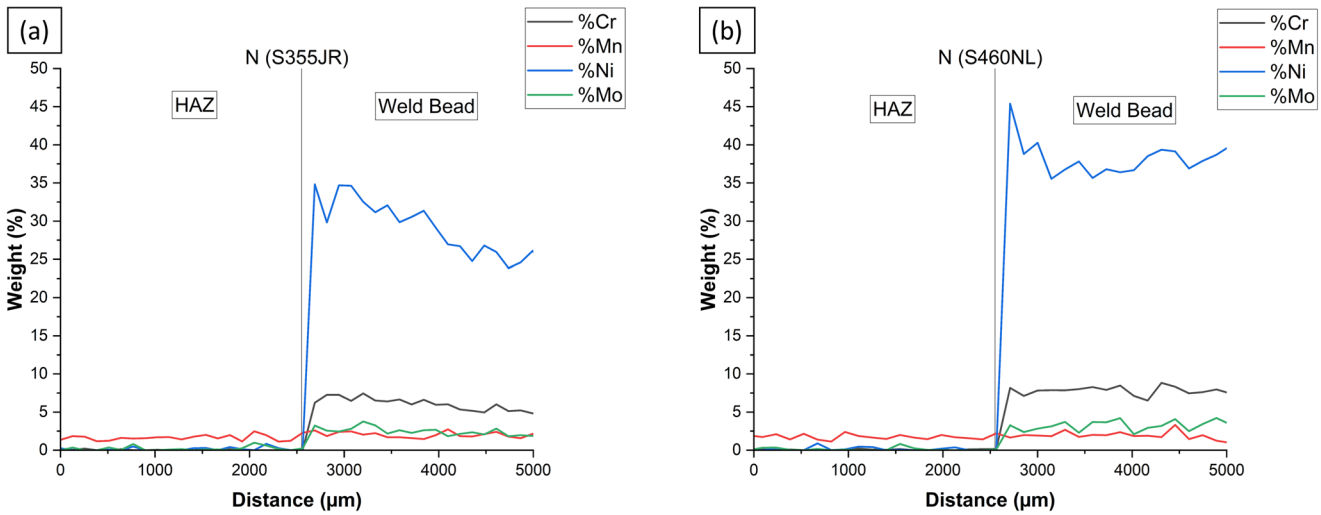

Fig. 10 | EDS line scan. Data across the weld bead/HAZ interface generated with the N electrode **a** on S355JR, **b** on S460NL.

Table 1 | Pitting resistance equivalent number of the weld beads generated with the austenitic stainless steel and the nickel-based electrodes

		PREN
FINOX 4519 AC—Kjellberg		28
Cr-Ni - voestalpine böhler	S355JR	25
AquaSan—ESAB/Surweld U.S.		27
FINOX 4519 AC—Kjellberg		30
Cr-Ni - voestalpine böhler	S460NL	26
AquaSan—ESAB/Surweld U.S.		26

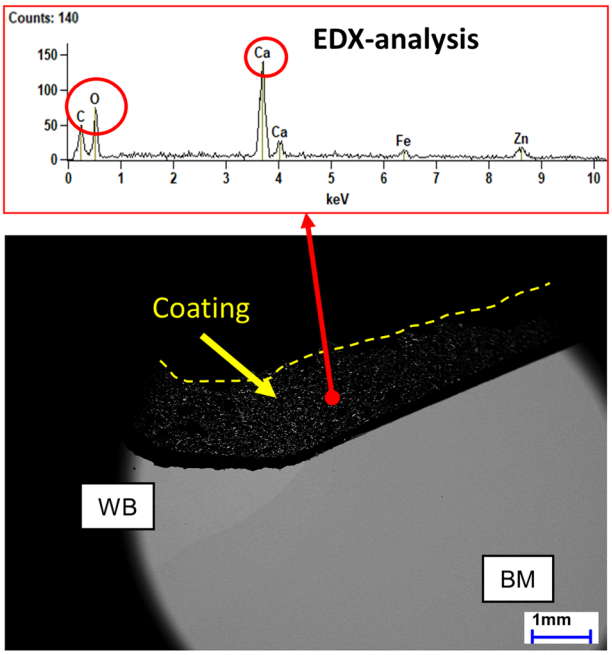

Fig. 11 | Coated samples. Coated austenitic stainless steel weld bead (on S355JR) after 360 days of aging in the Baltic Sea. (BM base material / WB weld bead).

arc voltage control (AVC), the arc remains at a constant length during the entire welding process. The electrode was positioned vertically at 90° to the workpiece (welding position PA). A welding power source developed for underwater welding (*AMT Maschinen- und Gerätetechnik GmbH*) and coated electrodes were used. The electrodes were connected to the negative pole of the welding power source (DCEN). The welding speed was kept constant at 0.2 m/min, and the current, voltage, and heat input (*E*) values used are shown in Table 2.

The samples were T-joints of 100 mm length. The surface ratio between the base metal and the fillet was 40:1. Four different electrodes were used, and their designations are given. All electrodes used, except for the Cr-Ni—voestalpine Böhler (A1) are commercially available. Among the electrodes used, only the FINOX 4519 AC (A2) electrode is not specifically developed for underwater welding and was, therefore, coated manually with a varnish. Two different base metals in the form of 10 mm thick plates were used, with compositions given in Table 3. The carbon equivalent ($C_{eq(IIW)}$) was calculated using the equation adopted by the International Institute for Welding.

Visual inspections of all joints revealed no major defects. Energy-dispersive X-ray spectroscopy (EDS) technique was then used to perform EDS line scan analysis over a length of 6 millimeters of the weld bead, HAZ, and base metal. Samples varied between the four electrodes used (Table 4) and the two different steel grades (Table 3). Half of each group of samples were coated after welding. Samples were processed according to DoE (Full Factorial Design), as shown in Fig. 13.

Corrosion tests (Baltic Sea)

The samples were divided into four packages of 16 samples each, resulting in a total of 64 samples. The net bags were placed in the Baltic Sea at Kiel - Germany (54°21'27.3"N 10°08'34.2"E) (Fig. 14), and were hung by a rope at a water depth of 4 meters.

The samples were placed in the Baltic Sea on November 10, 2021. The first bag was removed from the water after 60 days submersed (Fig. 15), the second after 180 days, the third after 360 days and the fourth after 547 days (Fig. 16).

According to meteorological data[49], the temperature variations in the Baltic Sea are shown in Table 5.

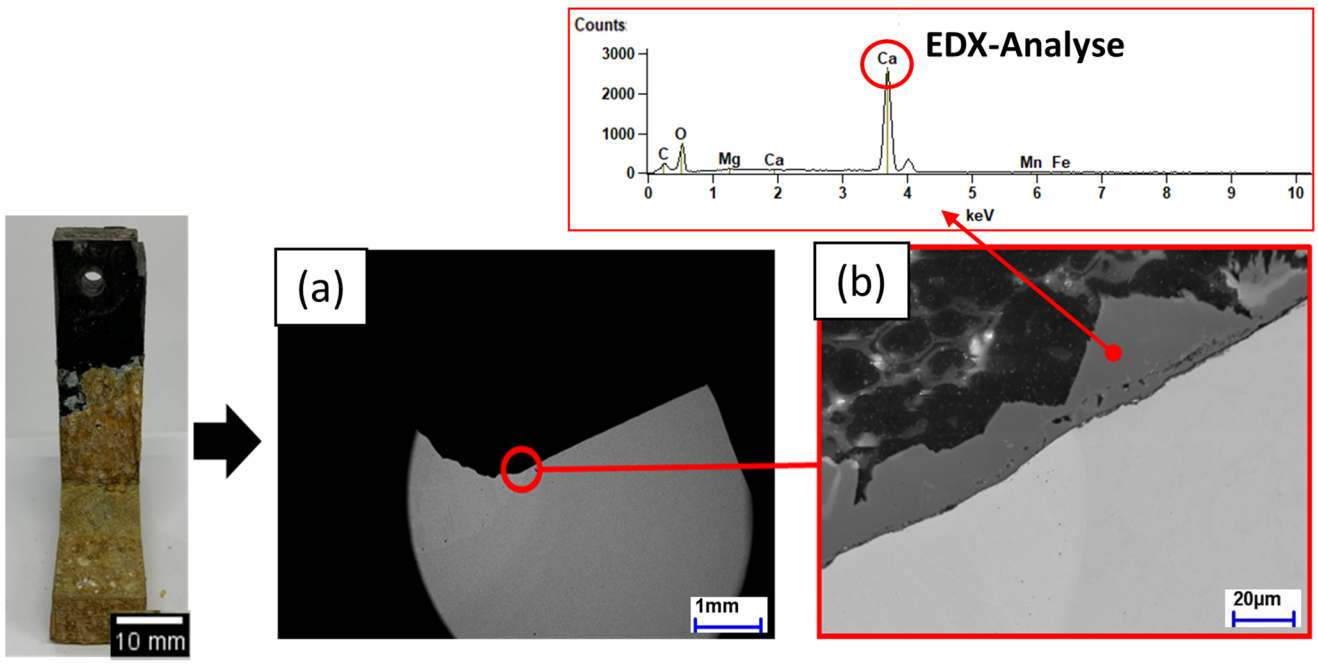

Fig. 12 | ICCP tests. a Sample after the Impressed Current Cathodic Protection test, **b** deposited layer with composition corresponding to $CaCO_3$ (A2 Electrode (On S355JR)).

After the corrosion tests, the samples were prepared metallographically following the guidelines of ISO/TR 20580:2022 37, and were etched with a 5% HNO_3 Nital solution.

Table 2 | Welding parameters and heat input; designations are based on the resulting weld metal structure (Nickel, Fe-austenite, Ferrite)

Electrode	Welding current, A	Arc voltage, V	Heat Input, J/mm	Designation
AquaSan Ni 50—ESAB/Sur-weld U.S.	100	31	931	N
Cr-Ni—voestalpine Böhler	120	33	1189	A1
FINOX 4519 AC (coated)—Kjellberg	110	32	1057	A2
AQUAWELD—Kjellberg	140	30	1261	F

Table 3 | Chemical composition of the base metals in wt.%

Base Metal	C	Mn	P	S	Si	Al	Cu	$C_{eq(IIW)}$
S355JR	≤0.24	≤1.6	≤0.035	≤0.035	≤0.55	–	≤0.55	0.37
S460NL	≤0.20	1–1.70	≤0.025	≤0.020	≤0.60	≥0.02	≤0.55	0.45

Corrosion tests (salt spray chamber)

Another group of samples, prepared identically to those submerged in the Baltic Sea, were tested in a salt spray chamber. *DIN EN ISO 9227* describes the procedure used for these tests[50]. Specifically, the samples were stored in the chamber in which a 5% NaCl solution with a controlled pH value was continuously nebulized at a temperature of 35 ± 2 °C. The solution flowed at 500 ml/h and the samples were stored for 720 h (30 days).

Electrochemical tests

Polarization curves were recorded using a Gamry Reference 600 potentiostat. The measurements were made according to ISO 17475[38]. An electrochemical pen (EC-Pen - IPS Elektroniklabor GmbH & Co. KG) was used, composed of a platinum counter electrode and a reference electrode (Ag/AgCl electrode)(1 M KCl). The base metal was connected to the working electrode terminal. The tip of the EC-Pen probed an area of 1 mm^2. The cross-section of the specimens was prepared metallographically. Polarization curves were obtained for the weld beads after dilution with base metal (only one weld bead), the HAZ, and the base metal. The electrode tip was placed in the area of interest, and three polarization curves were measured for each condition. The corrosion potential (E_{corr}) was obtained by Tafel extrapolation. The E_{corr} values reported represent the average between the three values obtained. The scan rate was 0.4 mV/s, and the scan covered a range of 0.2 V around E_{corr}.

Table 4 | Chemical composition and microstructure in wt.%

Electrode	C	Si	Mn	Mo	Ni	Cr	Fe	Microstructure
N	0.04	0.3	2.4	6.6	63.8	13	Balance	Austenitic/nickel alloy
A1	0.06	0.5	0.6	3.0	25	16	Balance	Austenitic/stainless steel
A2	0.03	0.9	1.5	4.5	25	20	Balance	Austenitic/stainless steel
F	0.05	0.25	0.5	0.5	-	-	Balance	Ferritic/non-alloyed steel

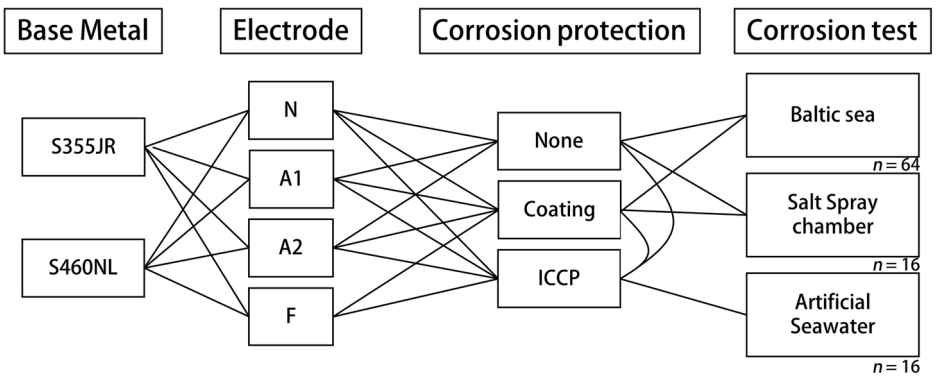

Fig. 13 | DoE. Schematic representation of the analyzed samples.

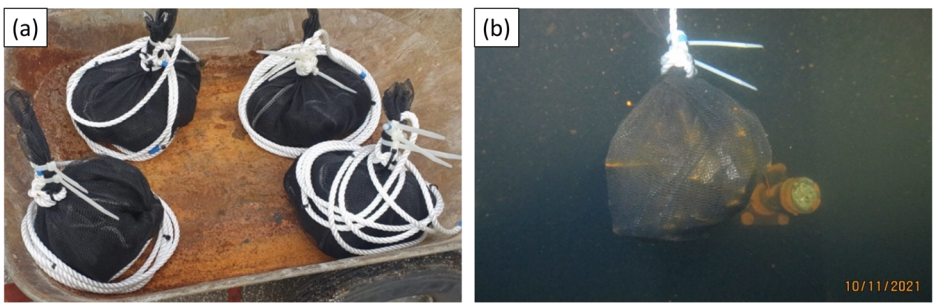

Fig. 14 | Corrosion tests. a nets with samples, **b** net containing a group of samples at 4 meters depth in the Baltic Sea.

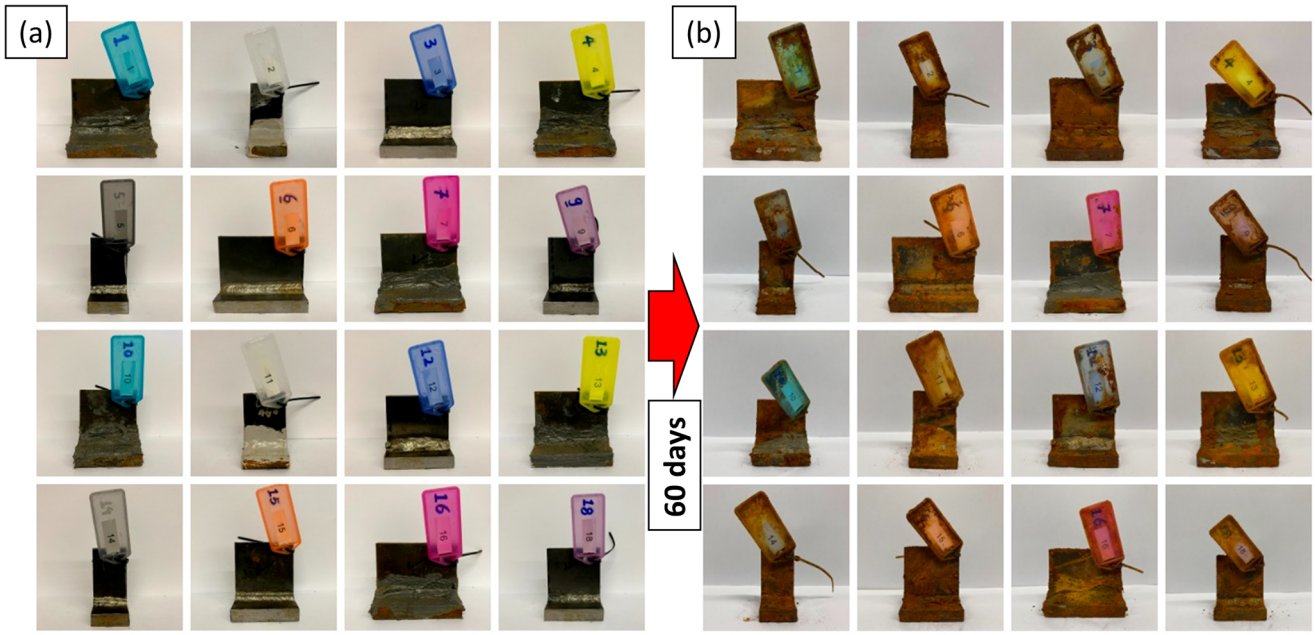

Fig. 15 | Corrosion tests. Samples before **a** and after **b** 60 days submerged in the Baltic Sea.

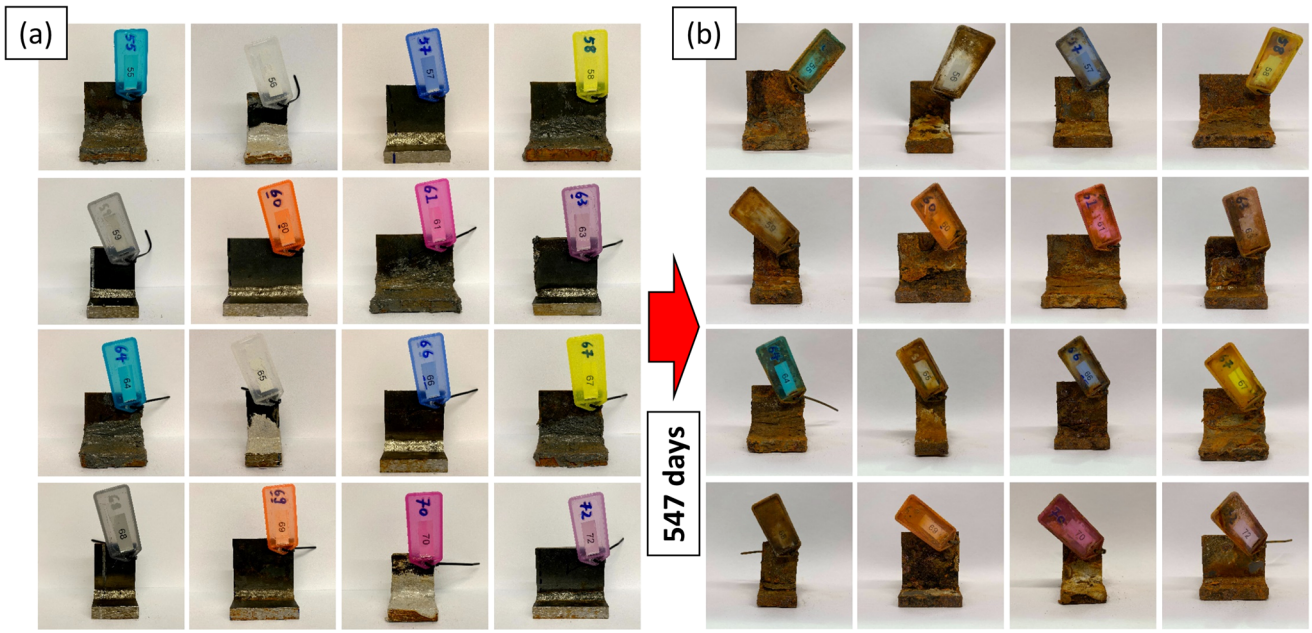

Fig. 16 | Corrosion tests. Samples before **a** and after **b** 547 days submerged in the Baltic Sea.

Table 5 | Season of the year, average temperature, and pH[49]

Season	Average temperature (°C)	pH
Winter	3.2	8 to 8.5
Spring	8.4	8 to 8.5
Summer	16.6	8 to 8.5
Autumn	12.5	8 to 8.5

Corrosion protection (coating)

The coating was intended to isolate the contact between the weld bead and the electrolyte (seawater), and thus prevent against galvanic corrosion. A 2-component epoxy-based coating for underwater application was used[29]. The coating was applied to the welded samples using a brush. The curing process of the coating was carried out underwater for 48 hours and the thickness of the coating was measured with the help of a thickness gauge at multiple points of the sample. In order to achieve a coating thickness between 0.3 and 1 mm as recommended by the manufacturer, an additional layer had to be applied to some samples and left subsequently for an additional 48 hours of curing.

Corrosion protection (ICCP)

The ICCP system was set up to mimic an ICCP system as employed offshore structures. The ICCP system consisted of an anode, a rectifier,

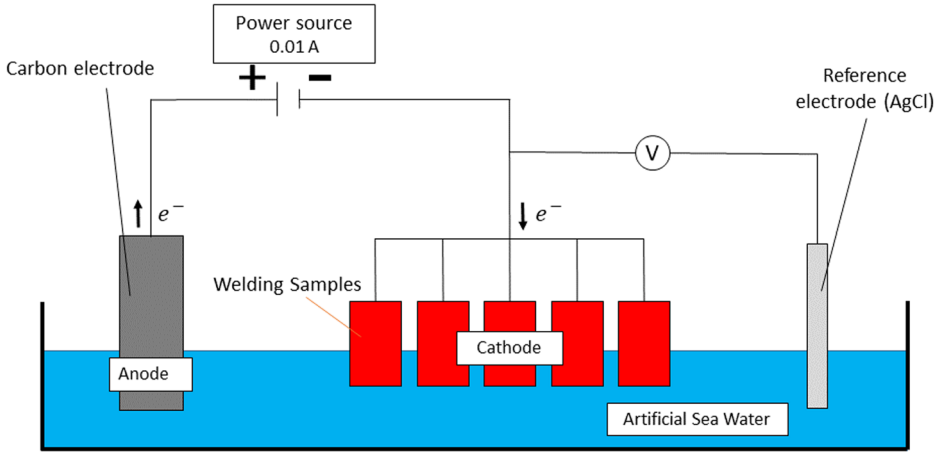

Fig. 17 | ICCP system. Setup as used to mimic a system as used on offshore structures.

and a reference electrode. A graphite electrode was used as the anode, while the samples were connected to the negative terminal acting as a cathode. The NACE-SP-0169 standard was followed for evaluation[32]. Figure 17 schematically shows the configuration of the ICCP system setup. A total of 16 samples were subjected to the test, as shown in. A 50-liter solution of DIN artificial seawater, prepared according to test standards[51,52] was used as the electrolyte. The solution was topped up to the initial level (50 liters) once every 30 days, and stirred once a day on weekdays.

Data availability

Data are available upon request to the corresponding author.

Received: 20 November 2023; Accepted: 26 April 2024;
Published online: 11 May 2024

References

1. Rowe, M. & Liu, S. Recent developments in underwater wet welding. *Sci. Technol. Weld. Join.* **6**, 387–396 (2001).
2. Lendiel, I., Klett, J., Schmidt, E., Vaccari, L. & Hassel, T. Manufacture and investigation of twochamber flux-cored wires for continuous underwater wet welding. *Weld. Cutt.* **21**, 296–302 (2022).
3. ASM International Handbook Committee (ed.). ASM metals handbook volume 6 - Welding, Brazing and Soldering (ASM International, 1993).
4. Hassel, T., Keßler, O., Klett, J., Reich, M. & Schumacher, P. Werkstofftechnisch basiertes Modell für die Simulation des Unterwasserschweißens. *Schweiß. Schneid.*, **71**, 513–519 (2019).
5. Łabanowski, J. Development of under-water welding techniques. *Weld. Int.* **25**, 933–937 (2011).
6. Pope, A. M., Teixeira, J. C. G., dos Santos, V. R., Paes, M. T. P. & Liu, S. The effect of nickel on the mechanical properties of high-oxygen underwater wet welds. *J. Offshore Mech. Arct. Eng.* **118**, 165–168 (1996).
7. Omajene, J.E Fundamental difficulties associeted with underwater wet welding. *Int. J. Eng. Res. Appl.* **6**, 26–31 (2014).
8. Kong, X. et al. Measurement and analysis of the diffusible hydrogen in underwater wet welding joint. *MATEC Web. Conf.* **39**, 3004 (2016).
9. Świerczyńska, A., Fydrych, D. & Rogalski, G. Diffusible hydrogen management in underwater wet self-shielded flux cored arc welding. *Int. J. Hydrog. Energy* **42**, 24532–24540 (2017).
10. M. D. Rowe, T. W. Nelson, C. Lippold. Hydrogen-induced cracking along the fusion boundary of dissimilar metal welds. *Weld. J.* **78** (1999).
11. Welding consumables - Covered electrodes for manual metal arc welding of non-alloy and fine grain steels - EN ISO 2560:2009. *DIN EN ISO 2560:2010-03*.
12. ISO 2560:2009 -Welding consumables - Covered electrodes for manual metal arc welding of non-alloy and fine grain steels, https://www.iso.org/standard/45947.html.
13. Klett, J. & Hassel, T. Influence of stick electrode coating's moisture content on the diffusible hydrogen in underwater wet shielded metal arc welding. *Adv. Mat. Sci.* **20**, 27–37 (2020).
14. Klett, J. et al. Control of the diffusible hydrogen content in different steel phases through the targeted use of different welding consumables in underwater wet welding. *Mat. Corr.* **8**, 11 (2020).
15. Klett, J., Wolf, T., Maier, H. J. & Hassel, T. The applicability of the standard DIN EN ISO 3690 for the analysis of diffusible hydrogen content in underwater wet welding. *Materials* **13**, 3750 (2020).
16. Fydrych, D. & Tomków, J. & Świerczyńska, A. Determination of diffusible hydrogen content in the deposited metal of rutile electrodes. *MAFE* **39**, 43 (2013).
17. Klett, J. et al. Effect of the water depth on the hydrogen content in SMAW wet welded joints. *SN Appl. Sci.* **2**, 25 (2020).
18. Pircher, H. & Großterlinden, R. Hydrogen induced corrosion of low alloy steels in hydrous media. *Mat. Corr.* **38**, 57–64 (1987).
19. ASTM G59 - Standard test method for conducting potentiodynamic polarization resistance measurements (1999).
20. Zaki Ahmad. Principles of corrosion engineering and corrosion control (Elsevier, 2006).
21. Hack, H. P. Galvanic corrosion (ASTM Int., 1988).
22. ASM International Handbook Committee (ed.). ASM Met. Handb. Vol. 13 - Corrosion.
23. Revie, R. W. & Uhlig, H. H. Uhlig's corrosion handbook. 3rd edn. (Wiley-Blackwell, 2010).
24. Kong, X. F., Lv, J., Gao, N., Peng, X. & Zhang, J. An experimental study of galvanic corrosion on an underwater weld joint. *J. Coast. Res.* **84**, 63–68 (2018).
25. Bai, Q. et al. The influence of the corrosion product layer generated on the high strength low-alloy steels welded by underwater wet welding with stainless steel electrodes in seawater. *J. Ocean Univ. China* **16**, 49–56 (2017).
26. Mudali, U. K. & Pujar, M. G. Pitting corrosion of austenitic stainless steels and their weldments. *In*: Corrosion of austenitic stainless steels: mechanism, mitigation and monitoring, 74–105 (2002).
27. Frankel, G. S. Pitting corrosion of metals: a review of the critical factors. *J. Electrochem. Soc.* **145**, 2186 (1998).
28. Iberl, P., Alt, N. S. A. & Schluecker, E. Evaluation of corrosion of materials for application in geothermal systems in Central Europe. *Mater. Corros.* **66**, 733–755 (2015).
29. LESTIN & CO. Datasheet - LECO-UWB-S5 - coating system for wet substrates and application underwater, https://www.nemopowertools.at/en/item/itemdetails/leco-uwb-s5/18.

30. ISO/DIS 24656:2020 - Cathodic protection of offshore wind structures, https://www.iso.org/standard/79166.html.
31. Robert G. Kelly, John R. Scully, David Shoesmith & Rudolph G. Buchheit. Electrochemical techniques in corrosion science and engineering. *In:* Corrosion technology (CRC, 2002).
32. NACE International. NACE-SP-0169-2013 - control of external corrosion on underground or submerged metallic piping systems, http://zinoglobal.com/wp-content/uploads/2019/12/NACE-RP-0169-2002.pdf.
33. Gasol & Josep M. (Editor). Microbial ecology of the oceans (Wiley Blackwell, 2018).
34. Hinners, J., Hofmeister, R. & Hense, I. Modeling the role of pH on baltic sea cyanobacteria. *MDPI Life* **5**, 1204–1217 (2015).
35. Karoui, H. et al. Electrochemical scaling of stainless steel in artificial seawater: role of experimental conditions on CaCO3 and Mg(OH)2 formation. *Desalination* **311**, 234–240 (2013).
36. Ito, Y. and Bessyo, K. Weldability formula of high strength steels related to heataffected zone cracking. IIW Document, 576–568 (1968).
37. K. A. Yushchenko, Y. Y. Gretskii, S. Y. Maksimov. Study of physicometallurgical peculiarities of wet arc welding of structural steels. Underwater Wet Weld. Cut.: Int. Sem. Worksh. TWI North, 6–30 (1997).
38. Peethala, A. K., D, B. N., Rao, K, S. & G, R. Optimization of welding parameters and study on mechanical and pitting corrosion behavior of dissimilar stainless steel GTA welds. *Chem. Data Collect.* **43**, 100978 (2023).
39. Wang, J. et al. Influence of heat input on microstructure and corrosion resistance of underwater wet-welded E40 steel joints. *J. Mater. Eng. Perform.* **6**, 387 (2020).
40. Santillan, S. N., Valdez, S. B., Schorr, W. M., Martinez, R. A. & Colton, S. J. Corrosion of the heat-affected zone of stainless steel weldments. *Anti-Corros. Methods Mater.* **57**, 180–184 (2010).
41. Khatak, H. S. & Raj, B. (eds.). Corrosion of austenitic stainless steels: mechanism, mitigation and monitoring (Elsevier, 2002).
42. DIN EN ISO 11463 - Korrosion von Metallen und Legierungen — Richtlinien für die Bewertung der Lochkorrosion (ISO 11463:2020); Deutsche Fassung EN ISO 11463:2020 https://standards.iteh.ai/catalog/standards/cen/73367a48-a626-4700-9562-598e2908565b/en-iso-11463-2020.
43. ASTM G46 - guide for examination and evaluation of pitting corrosion, https://www.astm.org/g0046-21.html.
44. Feistel, R. et al. Density and Absolute Salinity of the Baltic Sea 2006–2009. *Ocean Sci.* **6**, 3–24 (2010).
45. Orozco-Cruz, R. et al. Effect of seawater pH variation on the growth of calcareous deposits and its effect on an impressed current cathodic protection system. *J. Solid State Electrochem.* **27**, 3003–3016 (2023).
46. Refait, P., Grolleau, A.-M., Jeannin, M. & Sabot, R. Cathodic protection of complex carbon steel structures in seawater. *CMD* **3**, 439–453 (2022).
47. Carré, C. et al. Electrochemical calcareous deposition in seawater. A review. *Environ. Chem. Lett.* **18**, 1193–1208 (2020).
48. Minola, M. et al. Laboratory studies of ship hull's material degradation scenarios to optimize a cathodic protection modelling software. *npj Mater. Degrad.* **7**; https://doi.org/10.1038/s41529-023-00341-w (2023).
49. Des Clics Nomades/SeaTemperature. Temperature of the Baltic Sea (Maasholm - Germany). Available at https://www.seatemperatu.re/europe/germany/maasholm/ (2023).
50. ISO 9227:2017 - Korrosionsprüfungen in künstlichen Atmosphären - Salzsprühnebelprüfungen, https://www.dinmedia.de/de/norm/din-en-iso-9227/264008940 (2017).
51. DIN EN 14868:2005-11, Korrosionsschutz metallischer Werkstoffe-Leitfaden für die Ermittlung der Korrosionswahrscheinlichkeit in geschlossenen Wasser-Zirkulationssystemen; Deutsche Fassung EN_14868:2005 (Beuth, 2005).
52. ASTM D 1141—98. Practice for the preparation of substitute ocean water, https://www.astm.org/d1141-98r21.html (2021).

Acknowledgements

This study was a part of the DVS research project IGF 21547 N funded by the AiF as a part of the program to support "Industrial Community Research and Development" (IGF) funded by the Federal Ministry for Economic Affairs and Climate Action on the basis of a decision of the German Bundestag. The authors thank Unterwasserkrause - Mutzeck GmbH, for help with the corrosion tests in the Baltic Sea, voestalpine Böhler Welding UTP Maintenance GmbH and Kjellberg Finsterwalde Elektroden und Zusatzwerkstoffe GmbH for supplying welding consumables for this study.

Author contributions

L.V.: for welding the samples and carrying out the tests, methodology and writing. J.K.: project design and implementation, T.S. and I.L.: test design and interpretation of results. T.H.: for project management, and H.J.M.: for writing and evaluation of the results. The authors would also like to thank P. M. Müller and T. Steinhoff for carrying out the induced current cathodic protection tests, the salt spray chamber tests and the polarization curves.

Funding

Open Access funding enabled and organized by Projekt DEAL.

Competing interests

The authors declare no competing interests.

Additional information

Correspondence and requests for materials should be addressed to Leandro Vaccari.